

Study on mechanical behaviors of column foot joint in traditional timber structure

Juan Wang^{1,2a}, Jun-Xiao He^{*1,2,4}, Qing-Shan Yang^{2,3b} and Na Yang^{1,2c}

¹School of Civil Engineering, Beijing Jiaotong University, Beijing 100044, China

²Beijing's Key Laboratory of Structural Wind Engineering and Urban Wind Environment, Beijing Jiaotong University, Beijing 100044, China

³School of Civil Engineering, Chongqing University, Chongqing 400044, China

⁴School of Computing, Engineering and Mathematics, Western Sydney University, Parramatta, NSW 2150, Australia

(Received March 27, 2017, Revised January 22, 2018, Accepted January 23, 2018)

Abstract. Column is usually floating on the stone base directly with or without positioning tenon in traditional Chinese timber structure. Vertical load originated by the heavy upper structure would induce large friction force and compression force between interfaces of column foot and stone base. This study focused on the mechanical behaviors of column foot joint with consideration of the influence of vertical load. Mechanism of column rocking and stress state of column foot has been explored by theoretical analysis. A nonlinear finite element model of column foot joint has been built and verified using the full-scale test. The verified model is then used to investigate the mechanical behaviors of the joint subjected to cyclic loading with different static vertical loads. Column rocking mechanism and stress distributions of column foot were studied in detail, showing good agreement with the theoretical analysis. Mechanical behaviors of column foot joint and the effects of the vertical load on the seismic behavior of column foot were studied. Result showed that compression stress, restoring moment and stiffness increased with the increase of vertical load. An appropriate vertical load originated by the heavy upper structure would produce certain restoring moment and reset the rocking columns, ensuring the stability of the whole frame.

Keywords: traditional Chinese timber structure; column foot joint; vertical load; column rocking; mechanical behavior; finite element model

1. Introduction

Wood has been used as a structural material since ancient times. Timber structures have been used widely around the world in history, notably in China, Korea, Japan and Europe (Li *et al.* 2016). As shown in Fig. 1(a) (Li 2009), traditional Chinese timber structure usually consists of a raised platform and a timber skeleton of posts and lintels supporting the roof. As can be seen in Fig. 1(b) (Liang 2011), the structure is typically an assembled structure with components connected by joints such as column foot joint, column head joint, beam-column joint with complex bracket and so on. Components have been shaped to form the tenon or mortise as shown in Fig. 1(c), and they are connected with other components to form a building frame. It is noted that joints are not mechanically connected with each other but are fixed by vertical load from heavy roof. Seismic ability of traditional Chinese timber structure is considered to be excellent due to

primarily large-diameter columns and beams and different kinds of flexible joints.

In a traditional Chinese timber structure, column foot joint connecting the upper structure and the platform transmits compressive force only without any tensile capacity. According to modern seismic design theory, it is known that when the restraints at the structural foundation are released, the structure will rock back and forth under earthquake inputs. This kind of structure restoring the original position through self-weight is defined as a rocking or self-centering structure. Previous researches have proved that the rocking of structures can reduce the seismic effect. It is noted that, column rocking plays major role in lateral resistance mechanism in traditional timber structure (Meano *et al.* 2007, Maeda *et al.* 2008) and column foot as the main load-carrying elements are vital for the stability of whole structure.

In recent years, researchers had renewed interests in traditional structures (Guan *et al.* 2008, King *et al.* 1996, Li *et al.* 2016, Maeno *et al.* 2007, Sandberg *et al.* 2000, Tadashi *et al.* 1999). Theoretical and experimental studies had been made and clarified the static and dynamic features of the column frame (Ban 1941, Hayashi *et al.* 1998, Kawai 1996, Maeno *et al.* 2004, Maeno *et al.* 2007, Maeda 2008). Lee *et al.* (2009) obtained the curve of rotation angles and restoring moment through local compression tests of wood elements. Zhang *et al.* (2013) derived the restoring moment of column foot joint with the assumption that the stress of column top is equal to that of column foot. Zhang and Xue

*Corresponding author, Ph.D.

E-mail: 14115289@bjtu.edu.cn

^aAssociate Professor

E-mail: juanwang@bjtu.edu.cn

^bProfessor

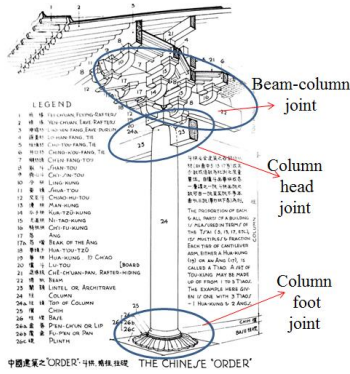
E-mail: qshyang@cqu.edu.cn

^cProfessor

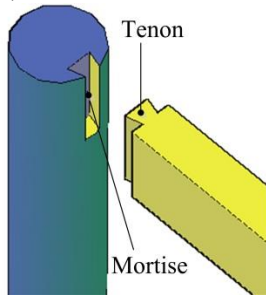
E-mail: nyang@bjtu.edu.cn



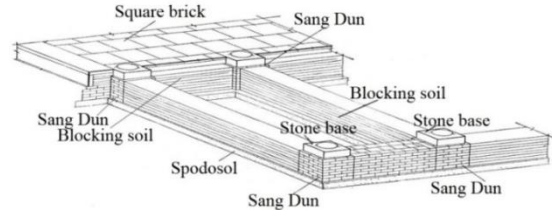
(a) Traditional Chinese timber structure



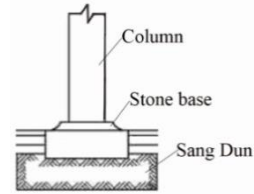
(b) The Chinese “order”



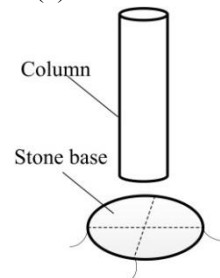
(c) Mortise and tenon joint



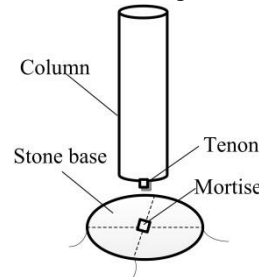
(a) Construction of platform



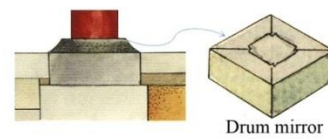
(b) Column foot



(c) Column foot without positioning tenon



(d) Column foot with positioning tenon



(e) Stone base called drum mirror



(f) Column foot in the Forbidden City in Beijing

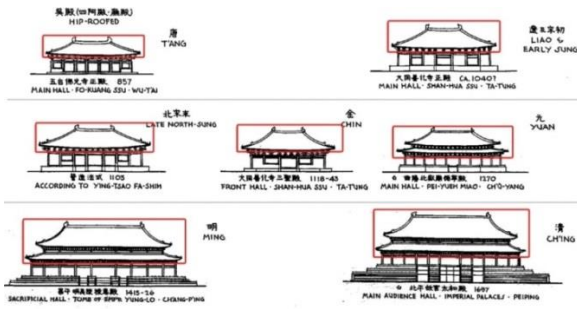
Fig. 1 Constructions of traditional Chinese timber structure

et al. (2011) studied the performances of vibration absorption and isolation of column foot joint by shaking table test. Maeno *et al.* (2004) analyzed the column rocking mechanism of traditional Japanese wooden frame. Existing researches showed that mechanical properties and stiffness characteristics of column foot joint in traditional Chinese timber structure were mostly indirectly analyzed basing on assumptions. And, few researches were focused on mechanical behaviors of column foot joint and the “column rocking” mechanism. Furthermore, most of the studies on structural analysis of timber structure have so far assumed the column foot and beam-column joints as rigid or pinned joint, without consideration of its semi-rigidity (Santana *et al.* 2009, Xue *et al.* 2017, Zhang *et al.* 2011). Especially, limited documentations were concerned with the behavior of the column foot joint subjected to repeated loading such as earthquake, and the influence of vertical load originated by heavy roof weight was out of consideration.

In this paper, the influence of vertical load on the mechanical behaviors of column foot joint in traditional Chinese timber structure was focused. Numerical

Fig. 2 Construction of column foot

simulations were used to investigate the behavior of column



(a) Development of the appearance of Chinese traditional timber structure



(b) Front view of the Imperial Palace



(c) Lateral view of Imperial Palace

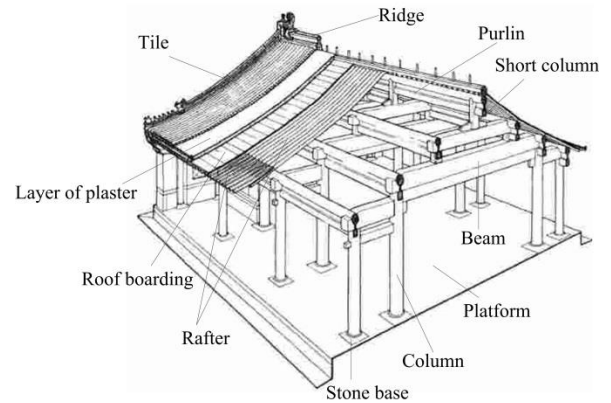
Fig. 3 Roof of traditional Chinese architecture

foot joint subjected to cyclic loading with applying different levels of vertical load. The column rocking mechanism and the stress distributions of the column foot joint were studied in detail. The characteristics of hysteretic capacity, equivalent radius, and stiffness degradation of the column foot are analyzed through the validated finite element model and the effects of vertical load on the hysteretic behavior were also discussed.

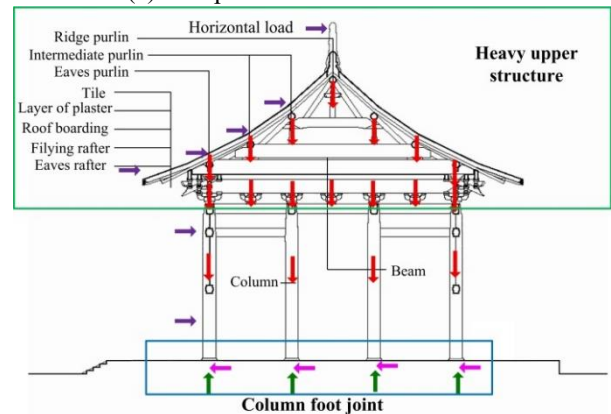
2. Mechanical behaviors of column foot

2.1 Typical column foot joints

The raised platform is one of the main architectural characteristics for Chinese traditional timber structure, and it composes of foundation, sang dun, blocking soil and stone base as shown in Fig. 2(a) (Tang *et al.* 2009). Sang dun on which the stone base buried is a kind of pier made of brick supporting the stone base and the column as shown in Fig. 2(b). Column is usually floating on the stone base directly as shown in Fig. 2(c) and (d). The most commonly used stone base with a concave shape shown in Fig. 2(e) (Wang 2006) is called drum mirror. Fig. 2(f) is a column with drum mirror in the Forbidden City in Beijing. Stone base protects column root free from damp. Area of drum mirror is usually larger than that of the cross section of column, so that stone base provides sufficient area for column slippage and in a way prevent collapse of column. According to the principle of static equilibrium, the biggest



(a) Composition of the timber frame



(b) Force flow chart of the frame

Fig. 4 Heavy roof in timber frame

shear force in column is equal to the friction force of column foot under horizontal force like earthquake or wind. Since the restraints at the structural foundation are released, this kind of column foot joint limits the maximum inner forces of the structure.

2.2 The functions of heavy roof

Fig. 3(a) shows the development of the appearance of Chinese traditional timber structure from Tang dynasty to Qing Dynasty around 1000 years (Liang 1991). It is noted that the proportion of the roof in the elevation tended to increase. Heavy roof with smooth curve and big eaves as shown in Fig. 3(b) and (c) is an invariant feature of Chinese traditional timber structure in spite of the changing times. The hipped roof not only has the basic function of water drainage, heat preservation and natural light adjustment etc., but also has certain structural functions.

The heavy roof is composed of a covering layer and a support layer. As shown in Fig. 4(a), the covering layer includes rafter, roof boarding, layer of plaster, tile, ridge and ridge ornament while the supporting layer is the roof frame consisting of purlin, beam and short column. The covering layer like a skin diaphragm improves the overall performance of roof. It has been analyzed that the weight of roof accounts for 75% to 85% of the whole building's weight. The weight of roof together with any external forces acting on the roof are passed onto the structure frame and

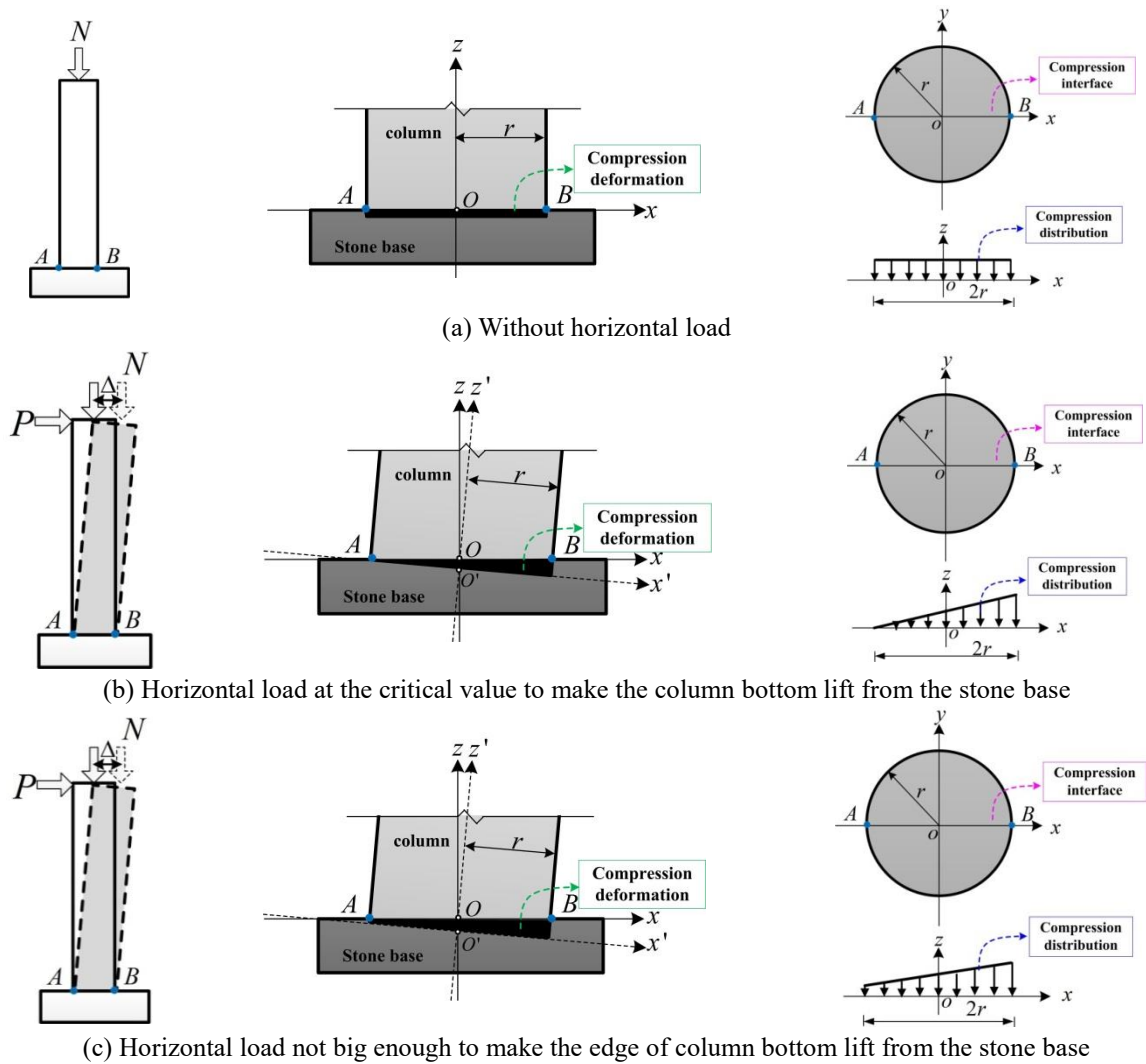


Fig. 5 Compression states of column foot without lifting

finally transferred to the foundation through columns as shown in the force flow chart in Fig. 4(b).

Different kinds of joints are not strongly connected but with certain geometric variability because of construction requirements and workmanship. The connections of components tend to be fixed in certain positions by the weight of heavy roof that induces friction and compression forces between interfaces of joints. Meanwhile, the weight of heavy roof plays an important role in resisting the slip of the structure and ensuring the stability of the whole frame.

2.3 Column rocking

Some Japanese researchers have done theoretical and experimental studies on the static and dynamic Characteristics of the column rocking for traditional wooden buildings in Japan (Kawai 1996, Maeno, *et al.* 2007, Maeda *et al.* 2008). It is found that both stiffness and strength of column rocking are depending on the building weight. Under horizontal load, the heavy roof would induce a large friction force, making column not easy to slip freely and on the other hand, it represents a large inertia force in the event of an earthquake causing substantial sway

(D'Ayala *et al.* 2008). Column rocking phenomenon exists in both Chinese and Japanese traditional timber structures. Periodic loads such as seismic actions would induce column rocking. Repeated lifting and setting of column foot make the structure frame be a self-centering structure through self-weight.

2.3.1 Compression states of column foot without lifting

If horizontal load is not big enough to make the edge of column bottom lift, the compression states of column foot can be expressed as Fig. 5(a)-(c) for different conditions respectively, where N , P and Δ denote vertical load, horizontal force and horizontal displacement of column top respectively; points A and B are the both ends of column bottom diameter and can be defined as the rotation fulcrum of column during rocking; x , y and z represent the initial coordinate system; while x' , y' and z' are the rotation coordinate system. O and O' are the centers of the column bottom before and after rotation respectively.

If horizontal load is zero, column bottom is fully in contact with the stone base, and the compression distribution of column bottom can be assumed uniform as

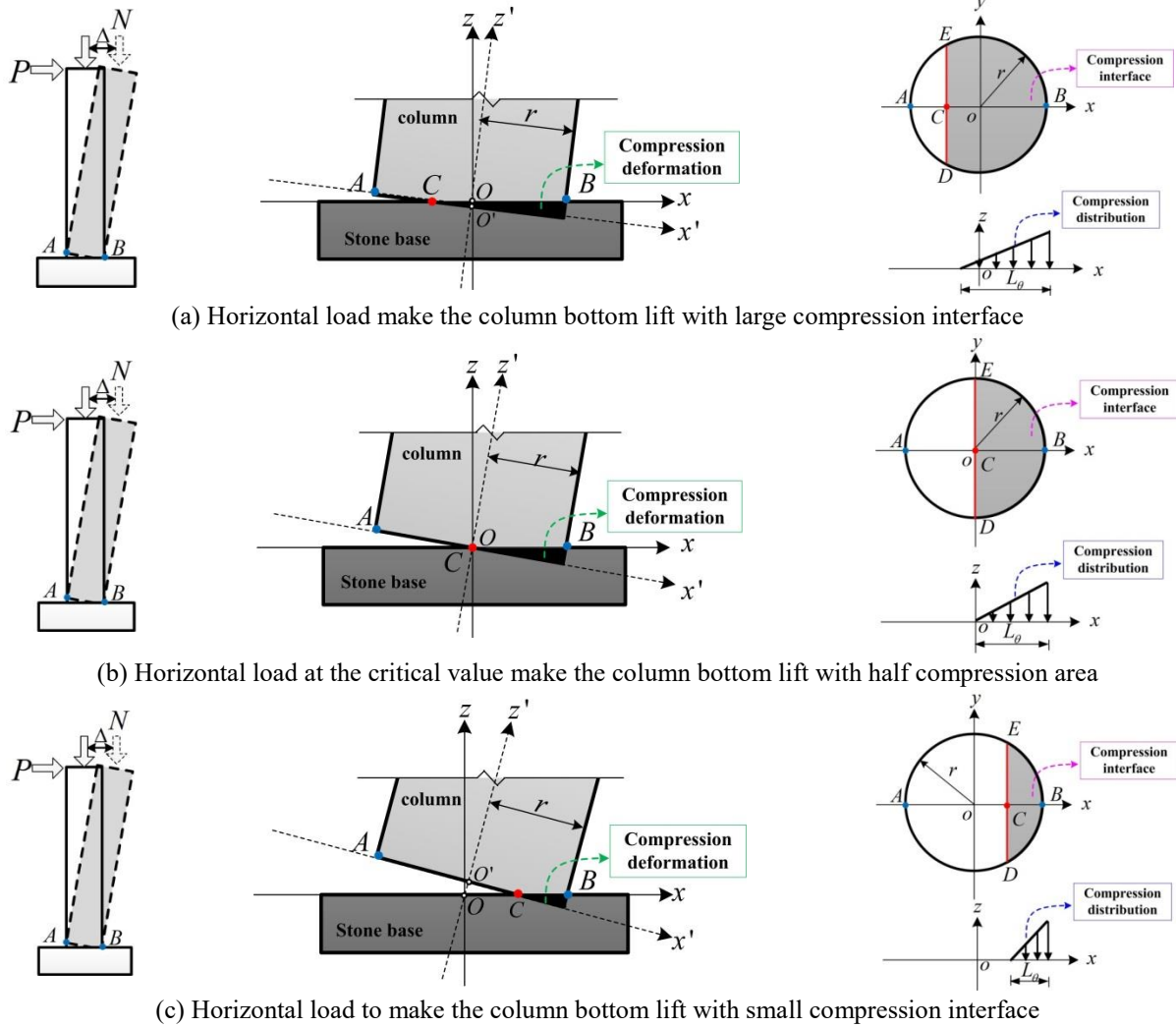
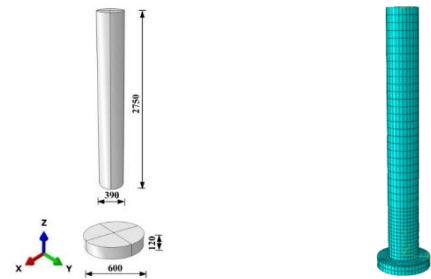


Fig. 6 Compression states of column bottom with lifting

shown in Fig. 5(a). If horizontal load is at the critical value to make the column bottom lift, the compression of column bottom is supposed to be simplified as a triangular distribution with zero compression at the side to be lifting and maximum compression at the opposite side as shown in Fig. 5(b). Fig. 5(c) shows the general condition with trapezoidal shaped compression distribution in between the two conditions shown in Fig. 5(a) and Fig. 5(b) respectively.

2.3.2 Compression states of column foot with lifting

If horizontal load is big enough to make the edge of column bottom lift, the compression states of column foot can be expressed as Fig. 6. The areas of contact and non-contact surfaces on the column bottom change with the rotation angle during rocking. In Fig. 6, DE is the boundary line between the contact and non-contact surfaces and point C is the center of DE . At the beginning of column lifting, most area of the column bottom is in contact with the stone base under small rotation angle. DE moves with the increase of rotation angle. Fig. 6(b) shows the critical condition that the horizontal load make the column bottom lift with half compression area and Fig. 6(c) is the condition



(a) Geometry of column foot joint (b) Mesh generation

Fig. 7 FEM of column foot

that column bottom lift with small compression interface. In either condition, the compression of column bottom is supposed to be simplified as a triangular distribution with zero compression at the boundary line and maximum compression value at the rotation fulcrum.

3. Finite element model

3.1 Model information

Experimental approach is essential to obtain first-hand

scientific data on mechanical behaviors of joints. However, if purely based on experimental work, it would be almost impossible to obtain deformations in contact areas of the joint. Therefore, it is necessary to develop a numerical model subjected to verification by the corresponding experimental results to simulate the joint by using finite element analysis. Thus, the mechanical behaviors of the joint can then be studied in detail.

A 3-D nonlinear finite element model of a column foot joint is developed using the commercial code ABAQUS. The simulated model is composed a traditional Chinese timber column (390 mm diameter, and 2750 mm height) and stone base (600 mm diameter and 120 mm height) as shown in Fig. 7(a). The dimensions are determined according to <Ying-tsao-fa-shih> (Li 2006), which is a technical treatise on engineering and architecture in the mid Song Dynasty of China. Fig. 7(b) shows the mesh generation of the joint where finer meshes are created on both interfaces and areas adjacent to the contact region. The discretization of both column and stone base consists of 8-node hexahedral finite elements (element C3D8R of ABAQUS), as this element can avoid the “hourglass” phenomenon in finite element computation.

3.2 Material properties

Column foot mainly depends on the timber parallel to grain to bear compression force under vertical load. Due to the stress on the weakening segment decreases little, and the stress-strain relationship can be simplified to the bilinear constitutive model (Chen *et al.* 2011). And, elastic-plastic model would be an appropriate constitutive model (Guan *et al.* 2008a, b). The timber in this experiment is Northeast pine with average density of 420 kg/m^3 , at 12% moisture content. Compressive tests were performed parallel to the grain to determine the axial compressive strength. The dimensions of the samples had a height of 40mm and a cross section of $20 \text{ mm} \times 20 \text{ mm}$. The samples are loaded in compression in a standard INSTRON-5552 machine at the cross-head speed of 2 mm/min . For axial orientation, 20 samples are tested. The average test results of elastic modulus, yield stress and Poisson ratio of the timber material are 8.856 GPa, 34.76 MPa and 0.3 respectively. The elastic modulus of stone base is around ten times larger than that of the timber material, and its Poisson's ratio is 0.19.

3.3 Boundary conditions

The boundary condition between stone base and foundation is assumed to be fixed. In such joint, the contact condition between column and stone base with friction is a non-linear problem and requires an appropriate method for the contact treatment. In this simulation, the contact pressure is calculated by using hard contact model implemented in ABAQUS. The Coulomb friction model is applied in which the static and dynamic friction coefficients are both set as 0.5. The loading process is slow so the difference between the dynamic and static friction coefficient is ignored.

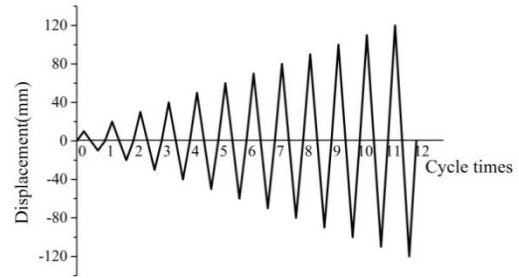
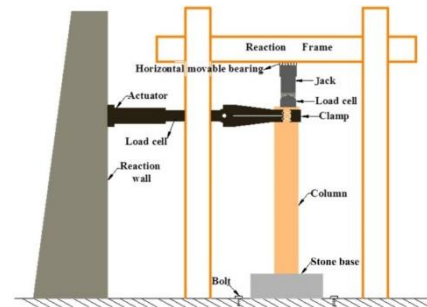
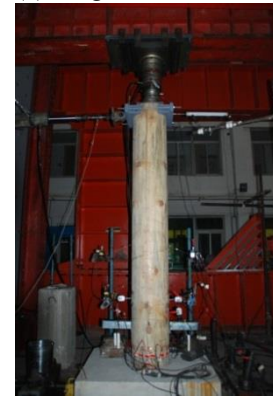


Fig. 8 Loading program of horizontal displacement



(a) Diagrammatic sketch



(b) Picture

Fig. 9 Loading apparatus

3.4 Loading program

Monotonic and cyclic loading tests based on displacement control method are performed on the joint. Each controlled displacement increases with 10mm displacement and cyclic loading for 12 times has been carried out as shown in Fig. 8. Vertical load simulated by means of lumped masses together with horizontal displacement is applied to the column top. In traditional Chinese timber building, the vertical load on column top is commonly around 23-43 kN, depending on different type of post-and-lintel construction. Therefore, three different amounts of vertical loads are set as parameters which are 20 kN, 35 kN and 50 kN respectively to analyze the influence of vertical load on the mechanical behaviors of column foot joint.

3.5 Experimental work

3.5.1 Introduction

Experimental work of a full-scale column with floating

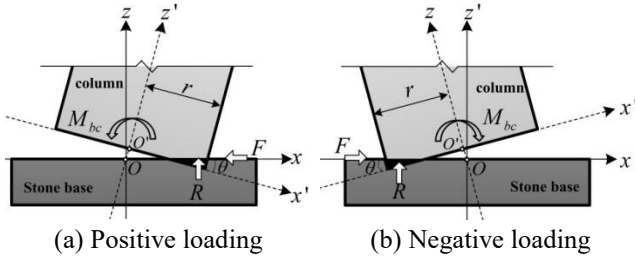


Fig. 10 Force state of column foot

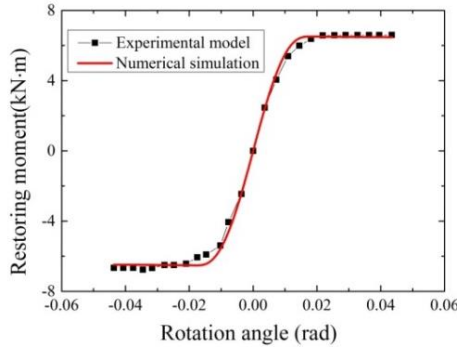


Fig. 11 Comparison between the experimental and numerical curves of restoring moment versus rotation angle under 35 kN vertical load

column foot joint based on <Ying-tsoo-fa-shih> (Li 2006) has been carried out. Fig. 9 shows the quasi-static test set up for the model. Column is floating on the stone base which is fixed on the laboratory ground. Vertical load (35 kN) applied on the column top is manually controlled by jack, which leads to give target constant force accurately throughout the experiment. Horizontal displacement is applied by MTS actuator to column top with the maximum displacement (120 mm) at one direction.

3.5.2 Validation of the finite element model

The restoring force due to column rocking is the major part of the total restoring force under small horizontal deformation (Maeno *et al.* 2004). In this study, rotational behaviors of column foot are mainly analyzed under the small horizontal deformation, and the partial compression at the top of the column can be neglected (Lee *et al.* 2009). Thus, vertical load can be assumed to be applied to the top center of column.

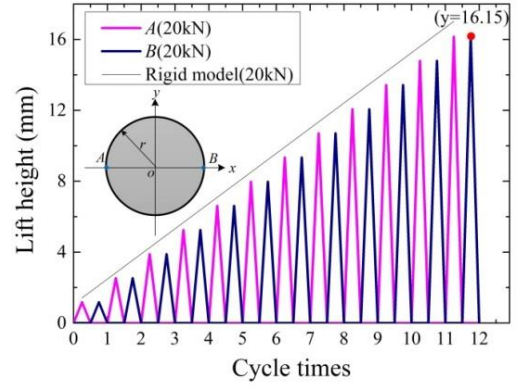
As shown in Fig. 10, vertical compression force R and friction force F are generated at the interface of column bottom during column rocking. It is noted that column is in the instantaneous equilibrium state. According to the moment balance at point O , the restoring moment of column foot M_{bc} is given by

$$M = Ph \quad (1)$$

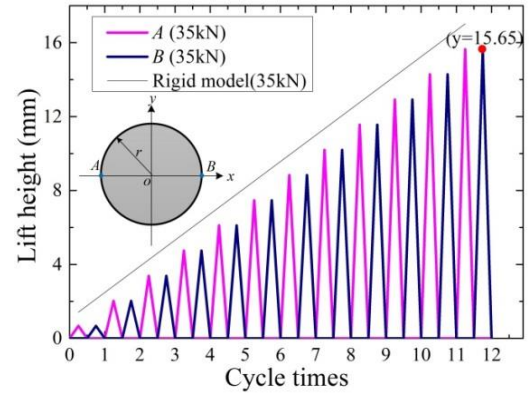
in which, h is the fang height.

Rotation angle of the column is expressed as

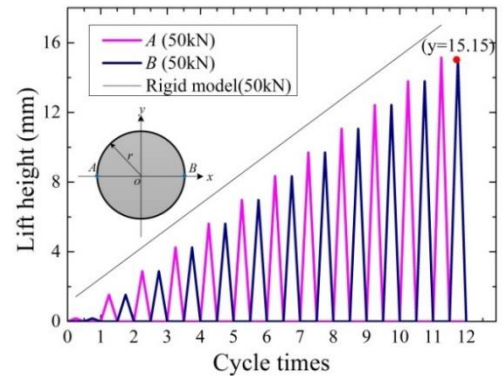
$$\theta = \tan^{-1} \left(\frac{\Delta}{h} \right) \approx \frac{\Delta}{h} \quad (2)$$



(a) Lifting heights of the two column edge points versus time under 20 kN



(b) Lifting heights of the two column edge points versus time under 35 kN



(c) Lifting heights of the two column edge points versus time under 50 kN

Fig. 12 Lifting heights of the two column edge points versus time under different vertical loads

The finite element model should be verified by the corresponding experimental results. It can be seen in Fig. 11 that good agreement of $M-\theta$ curves is obtained by finite element model and experimental test. The initial rotation stiffness seems to be linear. It is noted that column foot has a relatively high resistance to small rotation angle. Then, the rotation stiffness is almost invariable after 0.014 rad. Furthermore, restoring moment of column foot remains to be positive and active in preventing the column from collapse at the maximum rotation angle. It is found that column foot joint has certain amount of restoring moment

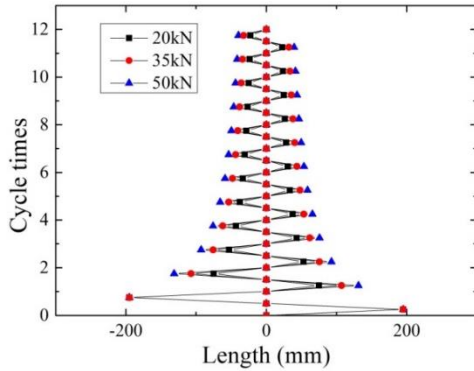


Fig. 13 Projections of the trace of boundary line DE versus time under different vertical loads

during column rocking to resist the overturning of structure under lateral load.

4. Results and discussion

4.1 Column rocking phenomenon

In the numerical analysis, column rocking is studied in detail. At the beginning of the cyclic loading, column rocking is not so obvious, because small displacement on the column top leads to relatively small rotation angle of the column. Fig. 12(a)-(c) show the lifting heights of the two edge points “A” and “B” at the column bottom in the whole cyclic loading process under the three different vertical loads respectively. It is noted that the two points lift alternately with the same pattern and same lifting height values, since the column and loading are both symmetrical. The lifting heights of “A” and “B” show a rising trend with the increase of displacement for different vertical loads. The black line denotes the lifting heights of the column edge points in rigid model, and its value is bigger than that of the un-rigid model under positive and negative loading. The lifting heights for point “B” in the last cycle for different vertical loads are signed in Fig. 12(a)-(c) respectively. It is found that the lifting height decreases with the increase of vertical load, because compression deformation increases with the increase of vertical load.

Fig. 13 shows the projection of the trace of boundary line DE between the contact and non-contact surfaces under different vertical loads respectively. The boundary line repeatedly alternates from one side to the other during rocking. In the initial stage of loading, the boundary line moves quickly to the edge of the column bottom and after that, it almost remains the same with the increase of rotation. It is found that the contact area between column and stone base increases with the increase of vertical load. Fig. 14 corresponds to the rotation states of column under 35 kN at the last cycle. It is noted that the column lifts and sets periodically at the contact surface during rocking.

4.2 Stress state of column foot joint

In this section, stress distributions on both contact

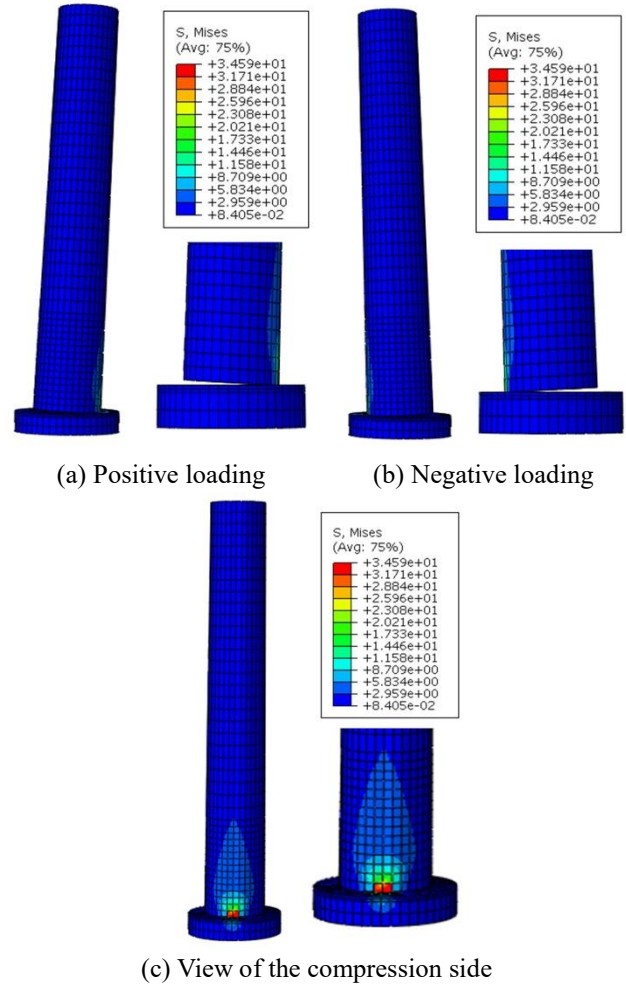


Fig. 14 Critical rotation states under 35 kN

surfaces and column edges adjacent to the contact regions are analyzed.

4.2.1 Stress distribution of the contact surface

4.2.1.1 Stress states of column foot without lifting

When the horizontal load is zero, the compression distributions of the contact surface under different vertical loads are shown in Fig. 15(a)-(c) respectively. It is found that the compression distribution is uniform and the compressive stress of the column bottom increase with the increase of vertical load. The critical states before lifting under different vertical loads are shown in Fig. 15(d)-(f) respectively. It is found that the compressive stress has the same pattern with nearly zero compression at the side to be lifted and maximum compression value at the opposite side. And, the compressive stress of column bottom increases with the increase of vertical load.

4.2.1.2 Critical states with column lifting

Fig. 16 shows the compression distributions of the three critical states with column lifting corresponding to the analysis shown in Fig. 6(a)-(c). Fig. 16(a)-(c) show the compression distributions of column bottom with large compression area under different vertical loads respectively.

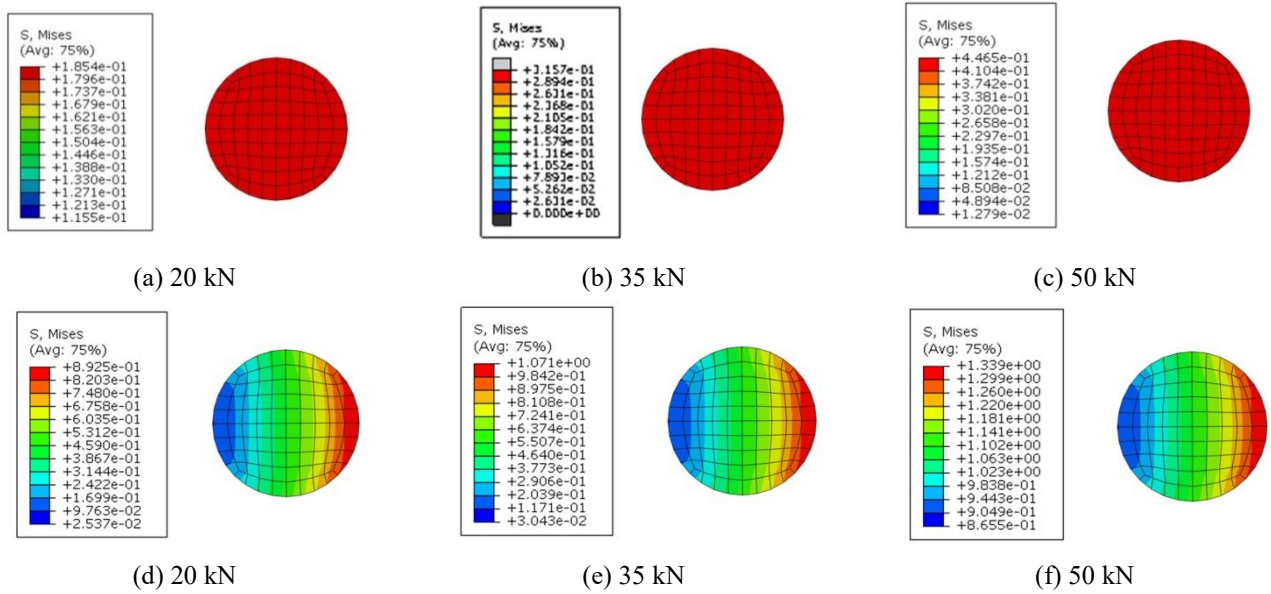


Fig. 15 Compression distribution of column bottom without lifting

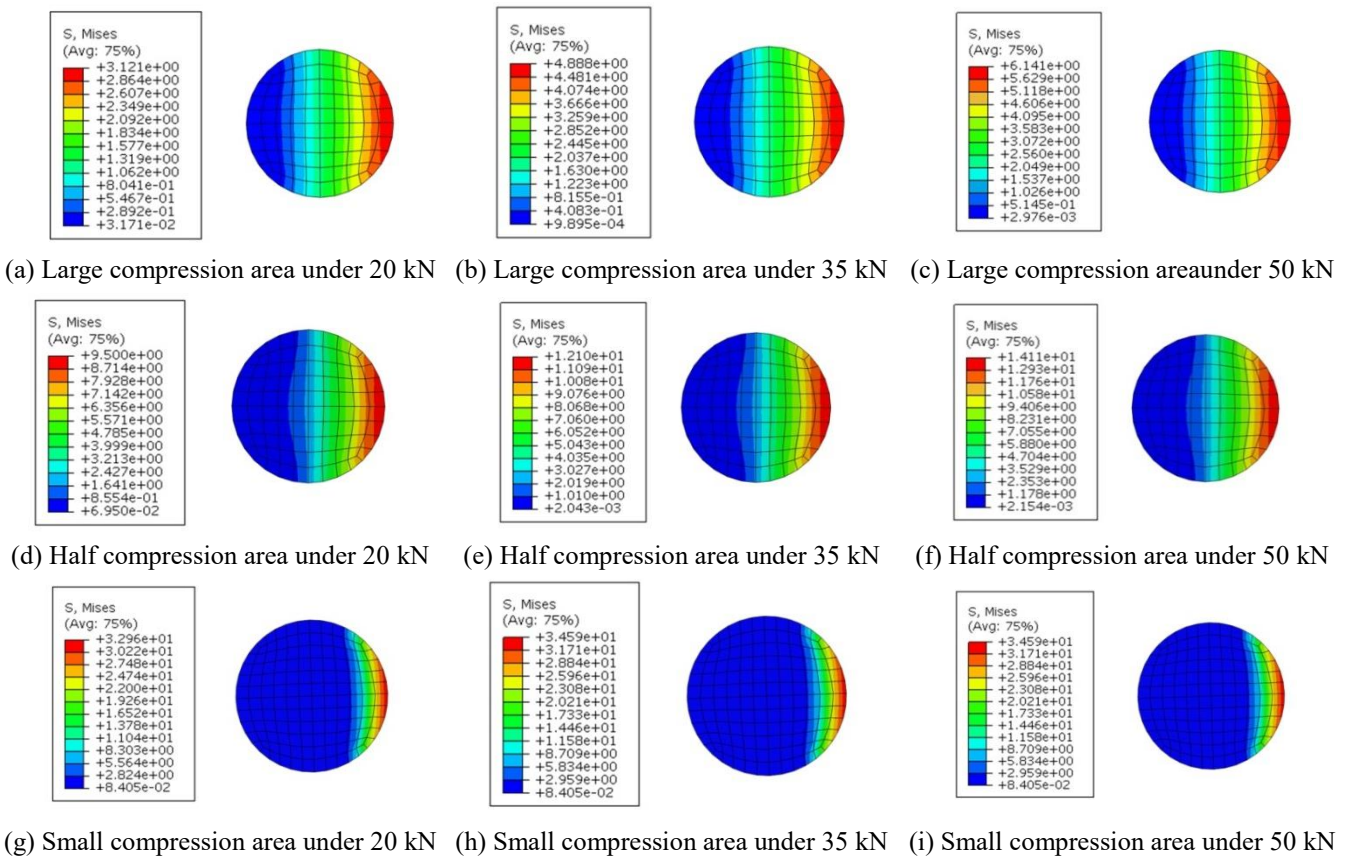


Fig. 16 Compression distribution of the column bottom with lifting

For all the vertical loads, compression is mainly in the large area of column foot at the initial stage of column lifting. The maximum compression occurs to the edge of column foot, and it increases with the increase of vertical load. Fig. 16(d-f) are the compression distribution of the column bottom with half compression area of column foot. Fig. 16(g-i) show the states of the column with lifting under

the controlled horizontal displacement of the last loading cycle. The maximum compression stress is equal to the yield stress parallel to the grain of column. It is founded from Fig. 16 that the compression area decreases with the increase of rotation angle. The boundary line between the contact and non-contact areas is almost straight and the stress increment is nearly uniform. The compression

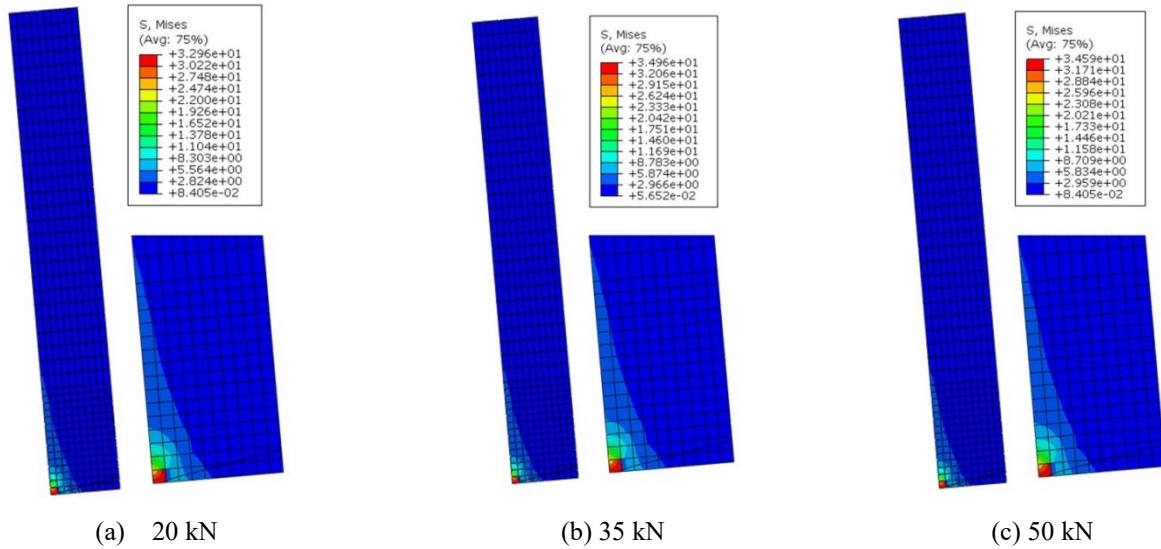


Fig. 17 Stress distribution of the column edges adjacent to the contact regions

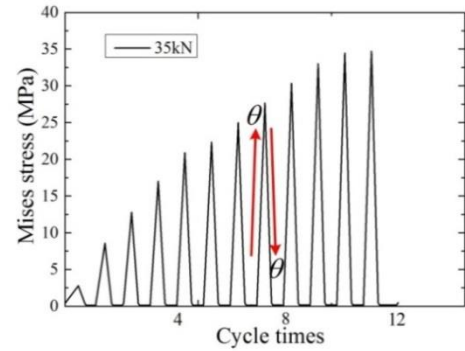
interfaces of the numerical model are consistent with those of analysis in Section 2.3. It is noted that, the compression distributions under negative loading are symmetrically consistent with those under positive loading shown in Fig. 16, since the rotation angles are of the same value at opposite directions.

4.2.2 Stress distribution of the column edges adjacent to the contact regions

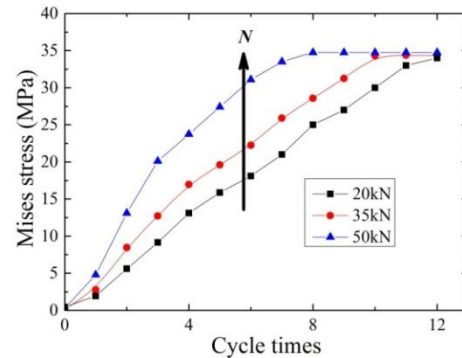
Stress distributions of the column edges adjacent to the contact regions under different vertical loads are shown in Fig. 17(a)-(c) respectively. It is found that the stress distribution at column edge adjacent to the contact regions is nearly triangular during column rocking with lifting. The maximum compressive stress locates at the edge of column foot while the minimum compression locates at the boundary between the contact and non-contact areas. The maximum stresses under different vertical loads are almost the same value, because the material at the column edge is yield at the last cycle. The numerical results of the stress state of column foot under cyclic loading prove that the analysis in Section 2.3.2 is rational.

4.2.3 Skeleton curve of compression stress of rotation fulcrum

Fig. 18(a) is the time-history of compression stress of rotation fulcrum “A” at column foot under 35kN vertical load. Compression stress is close to zero at the initial stage of loading and it increases with the increase of rotation angle at positive loading due to the increasing interaction between column and stone base. The compression stress reaches to the maximum value at the controlled rotation angle at the i th cycle. After that, it decreases during the process of column back to upright state. The controlled rotation angle at the i th cycle is smaller than that at the $(i+1)$ th cycle, so the maximum compression stress of rotation fulcrum is smaller than that at the $(i+1)$ th cycle. It is noted that the maximum compression stress reaches to the yield stress in the last two cycles.



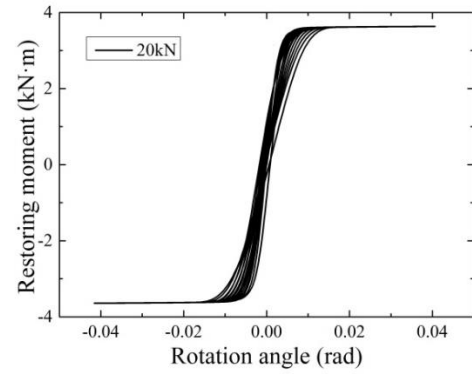
(a) Time-history curve of compression stress of rotation fulcrum “A” at column foot



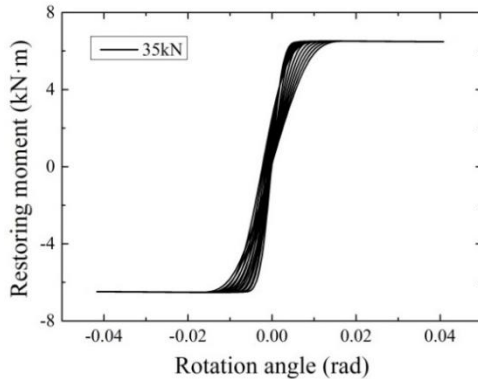
(b) Skeleton curves of compression stress of rotation fulcrum “A” at column foot under different vertical loads

Fig. 18 Compression stress of rotation fulcrum at column foot

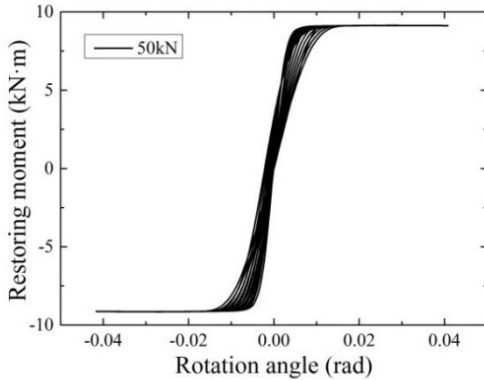
The peak points of time-history curve of compression stress under different vertical loads are connected with smooth curve respectively, and those are the skeleton curves shown in Fig. 18(b). Compression stress of column foot increases with the increase of vertical load. Column foot joint behaves elastic in the early stage of loading. Timber material reaches to the yield stress at the last, 10th and 8th cycle for 20 kN, 35 kN and 50 kN respectively. The larger



(a) 20 kN



(b) 35 kN



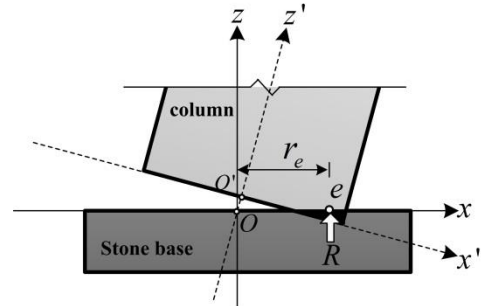
(c) 50 kN

Fig. 19 Hysteresis curves under different vertical loads

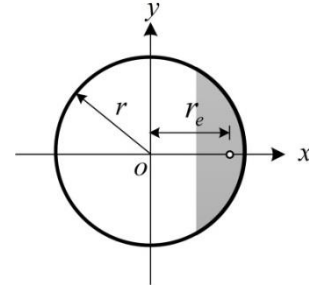
the vertical load is, the sooner yield phenomenon of column foot happens. It is noted that it is much easier for column foot to have material damages with larger vertical load.

4.3 Hysteretic behavior of column foot joint

The hysteretic curves of column foot joint shown in Fig. 19(a)-(c) for different vertical loads all have reverse Z shapes with pinch effect. The area of hysteresis curve which expresses the energy consumption increases gradually with the increase of rotation angle. The overall trend of hysteresis loop is anti-symmetric during loading. The curve is almost linear in the initial stage of loading. The restoring moment increases rapidly because the equivalent action center of compression force moving fast from the center to the edge of the column bottom. Hysteretic curve is no



(a) Vertical view of the column foot



(b) Cross section of the column

Fig. 20 Equivalent radius of column foot

longer linear after 0.01 rad. The restoring moment increases slowly, due to the compression interface and the equivalent action center of the compression force are close to the edge of column. Changing of the compression interface leads to small changing of the equivalent action center. The restoring moment almost remains the same value after 0.015 rad, because the compression interface is located at the edge of column foot and the changing of compression interface cannot cause the changing of equivalent action center of the compression force any more.

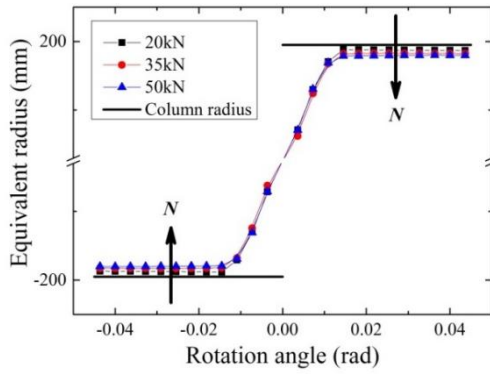
As shown in Fig. 19, the maximum restoring moments under 20 kN, 35 kN and 50 kN vertical loads are 3.64 kN·m, 6.52 kN·m and 9.12 kN·m respectively. The vertical load affects significantly on the restoring moment which is positively related to the compression force. The larger vertical load is, the greater restoring moment is. The compression deformation increases with the increase of vertical load. It is also explained why the area of hysteresis curve increases with the increasing of vertical load.

4.4 Equivalent radius of column foot

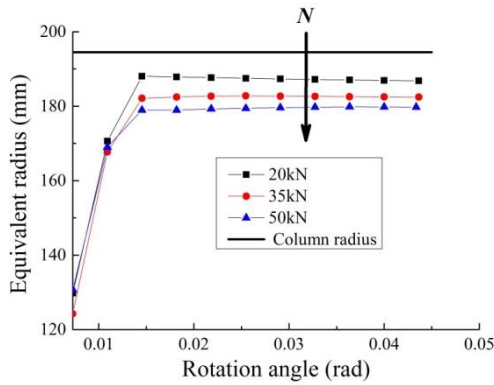
As shown in Fig. 20, the distance from the equivalent action center of the vertical compression force e to the rotation center O is defined as the equivalent radius of column foot, which is given by

$$r_e = \frac{M_{bc}}{N} \quad (3)$$

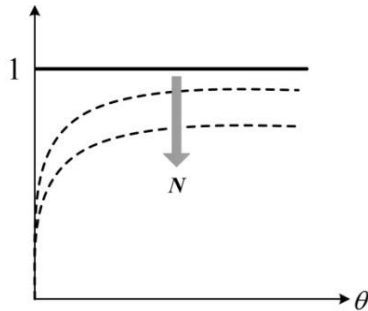
Fig. 21(a) shows the skeleton curves of equivalent radius under different vertical loads. It is found that the equivalent radius of column foot is always smaller than column radius. The equivalent radius is zero when the rotation angle is zero. At this time, the equivalent action center of the compression force overlaps with the center of



(a) Skeleton curves of equivalent radius under different vertical loads



(b) Partial enlarged drawing of the skeleton curves of equivalent radius



(c) Diagram of equivalent radius

Fig. 21 Skeleton curves of equivalent radius

column. Then the equivalent action center moves to the edge of column and the equivalent radius increases until the angle reaches to 0.015 rad. After that the equivalent radius becomes stabilized, because the compression interface is at the edge of column and no longer increases with the increase of rotation angle. Fig. 21(b) is the partial enlarged drawing of Fig. 21(a). It is found that the greater the vertical load is, the smaller the equivalent radius is. It is consistent with Lee's research result obtained by local compression tests of wood elements as shown in Fig. 21(c). The compression interface area increases with the increase of vertical load and the offset distance between the equivalent action center of compression force and the center of column decreases, so the equivalent radius reduces. The increase of vertical load would induce the increase of residual deformation of wood, such that leads to the material damages of column.

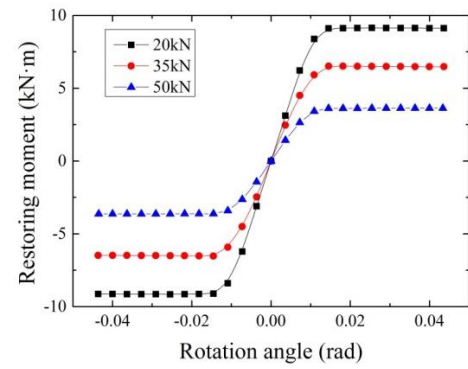


Fig. 22 Skeleton curves of $M \sim \theta$ under different vertical loads

4.5 Skeleton curve of column foot joint

It can be seen in Fig. 22 that the skeleton curves of column foot joint under different vertical loads all have a reverse Z shape and the curves are anti-symmetric at positive and negative loading. The restoring moment increases with increase of vertical load. In the initial stage, the rotation stiffness is linear. The skeleton curve is very steep such that small angle would cause rapid increase of restoring moment. The compression area moves to the column edge quickly and the rapid increase of equivalent radius leads to rapid increase of restoring moment. When the rotation angle reaches to 0.015 rad, the skeleton curve tends to be stable. Rotation stiffness decreases with the increase of lateral displacement. The skeleton curve has no descent segment in the whole loading process, indicating that the column foot joint is of good rotation ability.

4.6 Degradation of rotation stiffness

The secant rotation stiffness corresponding to each controlled rotation angle can be calculated as follows

$$k_i = \frac{|+M_i| + |-M_i|}{|+\theta_i| + |-\theta_i|} \quad (4)$$

where θ_i is the controlled rotation angle and M_i is the restoring moment at the i th cycle.

The degradation curves of rotation stiffness under different vertical loads are shown in Fig. 23. The trends of the three curves are almost the same. The rotation stiffness decreases with the increase of rotation angle, indicating that column foot joint has variable rotation stiffness. The initial rotation stiffness is relatively large and it obviously drops before the angle reaches to 0.022 rad. Although the rotation stiffness of column foot joint reduces with increase of rotation angle, it remains positive during loading to prevent column from collapsing. It is also found that in Fig. 23 that vertical load has a great influence on the initial rotation stiffness of column foot joint. Rotation stiffness increases with the increase of vertical load. The differences among the three curves are decreasing with the increase of rotation angle, indicating that the larger the rotation angle is, the smaller the influence of vertical load is.

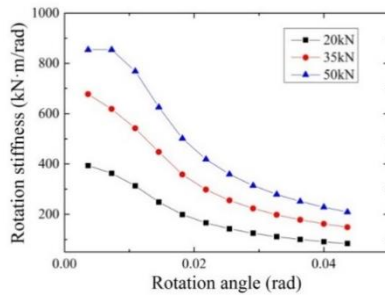


Fig. 23 Degradation curves of rotation stiffness under different vertical loads

5. Conclusions

This study focused on the mechanical behaviors of column foot joint with consideration of the influence of vertical load. Results of theoretical and numerical analysis reveals that vertical load originated by the heavy upper structure would induce a large friction force, making column not easy to slip freely and on the other hand representing a large inertia force causing column rocking under periodic horizontal inputs. Column is subjected to repeated lifting and resetting, with the rotation fulcrum and boundary line between the contact and non-contact areas alternating from one side to the other, making the structure as a self-centering structure. The lifting height of column foot during rocking decreases with the increase of vertical load. The more vertical load acting on the column foot, the more compression deformation occurs to the contact part.

The mechanical behaviors of column foot joint have been analyzed through the validated 3-D non-linear finite element model. Hysteretic curves appeared to be reverse Z shape with pinch effect. The equivalent radius is always smaller than column radius. The rotation stiffness decreases with the increase of rotation angle, showing semi-rigidity of the joint. The greater the vertical load is, the smaller the equivalent radius is; Compression stress, restoring moment and stiffness increases with the increase of vertical load. An appropriate vertical load originated by heavy upper structure would produce certain restoring moment and reset the rocking columns, ensuring the stability of the whole frame.

Acknowledgments

This work is supported by the National Natural Science Foundation of China (No. 51408038 and No. 51338001). The authors would like to thank the research project funding of the 111 Project of China (No. B13002), the National Key R&D Program of China (2017YFC0703505) and the Beijing Natural Science Foundation (No. 8151003). The financial support of the China Scholarship Council (CSC) is also acknowledged.

References

Ban, S. (1941), "Study on statics for structures of temple and

- shrine part-1", *Technical Papers of Annual Meeting, Architectural Institute of Japan (A.I.J)*, 252-258.
- Chen, Z.Y., Zhu, E.C. and Pan, J.L. (2011), "Numerical simulation of mechanical behaviour of wood under complex stress", *Chin. J. Comput. Mech.*, **28**(4), 629-635.
- D'Ayala, D.F. and Tsai, P.H. (2008), "Seismic vulnerability of historic Dieh-Dou timber structures in Taiwan", *Eng. Struct.*, **30**(8), 2101-2113.
- Guan, Z.W., Kitamori, A. and Komatsu, K. (2008), "Experimental study and finite element modelling of Japanese "Nuki" joints-part one: Initial stress states subjected to different wedge configurations", *Eng. Struct.*, **30**(7), 2032-2040.
- Guan, Z.W., Kitamori, A. and Komatsu, K. (2008), "Experimental study and finite element modelling of Japanese "Nuki" joints-part two: Racking resistance subjected to different wedge configurations", *Eng. Struct.*, **30**(2008), 2041-2049.
- Hayashi, T. (1998), "Restoring properties of Japanese traditional wooden frame", *Proceeding of the World Conference on Timber Engineering*, Presses Polytechniques et Universitaires Romandes, Montreux, Switzerland, August.
- Kawai, N. (1996), "Column rocking resistance in Japanese timber building", *International Wood Conference*.
- King, W.S., Yen, J.Y. and Yen, Y.N. (1996), "Joint characteristics of traditional Chinese wooden frames", *Eng. Struct.*, **18**(8), 635-644.
- Lee, D., Araki, Y. and Endo, T. (2009), "Modeling of column base for traditional timber buildings based on local compression experiments at contact surface between column base and foundation stone", *J. Struct. Constr. Eng.*, **74**(639), 865-872.
- Li, J. (2006), *Ying-Tsao-Fa-Shih*, China Bookstore Press, Beijing, China.
- Li, Q.L. (2009), *Penetration Through Walls: Study on the Classic Chinese Traditional Buildings*, Guangxi Normal University Press, Guangxi, China.
- Li, Y.Z., Cao, S.Y. and Xue, J.Y. (2016), "Analysis on mechanical behavior of dovetail mortise-tenon joints with looseness in traditional timber buildings", *Struct. Eng. Mech.*, **60**(5), 903-921.
- Liang, S.C. (1991), *A Pictorial History of Chinese Architecture*, China Building Industry Press, Beijing, China.
- Liang, S.C. (2011), *Chinese Architecture: Art and Artifacts*, Foreign Language Teaching and Research Press, Beijing, China.
- Maeda, T. (2008), "Column rocking behavior of traditional wooden buildings in Japan", *Proceedings of the 10th World Conference on Timber Engineering*, Miyazaki, January.
- Maeno, M., Suzuki, Y. and Ohshita, T. (2004), "Seismic response characteristics of traditional wooden frame by full-scale dynamic and static tests", *Proceedings of the 13th World Conference on Earthquake Engineering*, Vancouver, Canada, August.
- Maeno, M., Saito, S. and Suzuki, Y. (2007), "Evaluation of equilibrium of force acting on column and restoring force due to column rocking by full scale tests of traditional wooden frames", *J. Struct. Constr. Eng.*, 153-160.
- Sandberg, L.B., Bulleit, W.M. and Reid, E.H. (2000), "Strength and stiffness of oak pegs in traditional timber-frame joints", *J. Struct. Eng.*, **126**(6), 717-723.
- Santana, C.L.O. and Mascia, N.T. (2009), "Wooden framed structures with semi-rigid connections: Quantitative approach focused on design needs", *Struct. Eng. Mech.*, **31**(3), 315-331.
- Tadashi, N. and Kazuhiro, S. (1999), "Static and dynamic analyses of Japanese traditional timber buildings", *Proceedings of the Inter-National Seminar on Numerical Analysis in Solid and Fluid Dynamics*, Osaka, Japan, November.
- Tang, S.L., Yao, K. and Deng F.H. (2009), "Composite foundation construction technology in traditional timber structure", *Builder's Month.*, 10-13.

- Wang, Q.J. (2006), *Illustration Dictionary of Classical Chinese Architecture*, China Machine Press, Beijing, China.
- Xue, J.Y., Qi, L.J., Yang, K.Y. and Wu, Z.J. (2017), “Dynamic experimental study on single and double beam-column joints in steel traditional-style building”, *Struct. Eng. Mech.*, **63**(5), 617-628.
- Zhang, F.L., Zhao, H.T. and Xue, J.Y. (2013), “Lateral load-resisting analysis and experimental verification of ancient timber based on swing-columns principle”, *Ind. Constr.*, **43**(10), 54-60.
- Zhang, X.C., Xue, J.Y. and Zhao, H.T. (2011), “Study on Chinese ancient timber-frame building by shaking table test”, *Struct. Eng. Mech.*, **40**(4), 453-469.

CC